Version of Record: https://www.sciencedirect.com/science/article/pii/S0149197022002499
Manuscript_3d32a13471ba1ee34ca2e106df29dc7f

Near-Infrared Spectra and Molar Absorption Coefficients of Trivalent Lanthanides Dissolved in Molten LiCl-KCl Eutectic

Jeremy Moon[1] and Dev Chidambaram[1,2,*]
[1]Materials Science and Engineering
[2]Nevada Institute for Sustainability
University of Nevada, Reno, Reno, NV 89557-0388, USA.
* dcc@unr.edu

Abstract

Determining the concentration of the dissolved lanthanide species in LiCl-KCl eutectic salt is important to the development of pyrochemical reprocessing of used nuclear fuel. In this process, lanthanide fission products are found dissolved in the electrorefiner electrolyte in their trivalent oxidation state. The presence of dissolved trivalent lanthanides increases the liquidus temperature of the electrolyte mixture and can lead to the formation of insoluble oxide or oxychloride phases and must therefore be continuously monitored and controlled during the operation.

Absorbance spectroscopy is a promising method for continuous measurement of the concentration of lanthanides and other elements dissolved in the electrolyte. The absorption of light by elements is linearly proportional to the concentration of the element for relatively dilute solutions according to the Beer-Lambert law. Although measurement of the absorption of ultraviolet and visible range light by lanthanides in LiCl-KCl eutectic molten salt have been explored previously, near infrared (NIR) absorption spectroscopy has received far less attention. It may, however, provide a better analytical signal when insoluble phases are present due to less Raleigh scattering compared to shorter wavelength radiation. Additionally, it may allow for concentration determination for certain elements using NIR absorption features where UV and visible range features are overlapping with features from other species.

In this study, we report the UV-Vis-NIR spectra of the trivalent lanthanide chlorides of neodymium, samarium, and dysprosium in LiCl-KCl eutectic. Molar absorption coefficients are reported for analytically useful absorption maxima, with a focus on the molar absorption coefficients for NIR absorption maxima which have not been reported previously. Additionally, we observe a NIR-range absorption band of Nd^{3+} which was previously predicted but never experimentally observed. We compare the calculated crystal field levels to the newly observed absorbance band and find them to be in good agreement with previous predictions.

1. Introduction

Nuclear fission power generation provides a significant amount of the non-greenhouse gas emitting energy generated around the world. Further expansion of nuclear energy generating capacity is a viable pathway to meeting stringent greenhouse gas emissions target that will minimize increases in global average temperatures. Used nuclear fuel from low enriched light water reactor fuel contains approximately 95% reusable material; ^{235}U (~1%), ^{238}U (~93%), and Pu and various minor actinides (~1%) [1]. Pyrochemical reprocessing (pyroprocessing) of used nuclear fuel (UNF) can recover nearly all of remaining actinides, including transuranic elements, in used nuclear fuel and recycle these actinides into new nuclear fuel [2-4]. Pyroprocessing can incorporate commercial ceramic UNF though a head-end electrolytic reduction step in LiCl-Li_2O or can directly treat metallic UNF [2]. Following the head-end electrolytic reduction step for ceramic UNF, metallic UNF from either source is anodically dissolved in LiCl-KCl eutectic molten salt at 500 °C in the electrorefiner and actinides are deposited as metallic solids at cathodes. The electrorefined metallic actinides can then be reprocessed into metallic nuclear fuel rods or go through other processing steps for storage or reuse.

Efforts to optimize the pyroprocessing of UNF and integrate it into the nuclear fuel cycle have been ongoing; developing the understanding of the chemistry of the molten salt mixture is one such research area, as is developing additional means to monitor the composition of the molten salt mixture [5]. The molten salt in the electrorefiner is a mixture of the LiCl-KCl eutectic with dissolved actinides, lanthanides, and other fission products [2,3,6,7]. The addition of the dissolved UNF elements alters the thermochemical and thermophysical properties of the molten salt, with consequences to the efficiency of the electrodeposition of actinides and the operation of the system, as liquidus temperature rises [6]. The chemical state of the elements in the salt also dictates downstream processes to recondition and recycle the electrorefiner salt to minimize waste [2].

Absorbance spectroscopy is an analytical technique that measures the absorption of photons in a material from the ultraviolet (UV) through the visible (vis) and near infrared (NIR) energy ranges. Photons are absorbed by materials by promoting excitations of vibrational modes (with energies corresponding to IR or NIR photons), or electrons from the ground state to an unoccupied electronic state of higher energy (with energies corresponding to NIR, visible, or UV photons). These transitions can only be promoted by photons with energies equal to the energy difference between the ground and excited state, so by measuring the wavelength of photons absorbed, the energy of the transition is observed [8].

The probability of a photon being absorbed varies, for most practical purposes, linearly with the concentration of the species from which the transition originates and with the pathlength through the absorbing material for relatively low concentrations. This relationship is known as the Beer-Lambert law. The Beer-Lambert law allows for quantification of the concentration of an analyte, provided the molar absorption coefficient (ε) is known and the concentration of the unknown analyte lies in the linear region [9]. In a high-temperature, atmosphere-sensitive molten salt systems, absorption spectroscopy is a candidate to rapidly and non-destructively detect the concentration of analytes of interest within the system while minimizing the need to open the system for sampling or handling highly radioactive samples. The ability to monitor the composition of the salt using electrochemical and spectroscopic methods in the process vessel has been cited as a proliferation-resistance benefit of pyroprocessing [2].

In the present work, the absorption spectra of several trivalent lanthanides in LiCl-KCl eutectic molten salt are examined. Sm^{3+} and Nd^{3+} are directly relevant to pyroprocessing operations, while Dy^{3+} was selected to understand the behavior of a heavier lanthanide, even though it is not typically present in pyroprocessing molten salts. The lighter lanthanides are formed as fission products in nuclear fuel and dissolve into the electrorefiner salt alongside the actinide elements as trivalent species [2, 6]. In the Mk-IV electrorefiner at the fuel conditioning facility (FCF) at Idaho National Lab (INL), representative batches of fuel contained, for example, between 1.0-3.4 wt.% Nd, 0.3-0.7 wt.% Sm, 0.3-1.0 wt.% La, 0.6-1.9 wt.% Ce, and 0.3-1.0 wt.% Pr [6].

Previous investigations have examined the use of UV-vis spectroscopy to quantify trivalent lanthanides in LiCl-CsCl (60-30 mol. %) and LiCl-KCl eutectic at 500 °C. These studies reported the spectra of the trivalent lanthanides up to 900 nm in LiCl-KCl eutectic and reported molar absorbance coefficients [10, 11]. Additionally, early work by Banks and coworkers in the 1960s reported the UV and visible spectra for trivalent lanthanides in LiCl-KCl eutectic at 450 °C as well as several alkali fluoride and nitrate salts [12]. Molar absorption coefficients for Nd^{3+} in LiCl-KCl eutectic were also reported up to 900 nm by Fujii and coworkers in LiCl-KCl eutectic at 600 °C [13]. However, the NIR spectra for many of these elements have not appeared in the literature and no attempt has been made to determine molar absorption coefficients for the NIR absorption features of lanthanides dissolved in alkali halide molten salts. It should also be noted that none of the previous studies report accounting for the uncertainty in the abscissa (concentration) when determining molar absorption coefficients by least squares linear regression. To our knowledge none of the studies, other than the one by Fujii that report the Nd^{3+} molar absorption coefficients, provide the confidence level of their uncertainty estimates [10-13].

NIR transitions accessible for trivalent lanthanides up to 2400 nm are electronic in origin rather than hot band or combination band vibrational transitions seen in the NIR spectra of functional group or transition metal complexes [14-18]. These NIR transitions in lanthanides are therefore useful for concentration quantification in the same manner as UV and visible range transitions. To this end, the present investigation reports the UV-vis-NIR spectra of Sm^{3+}, Nd^{3+}, and Dy^{3+} and molar absorption coefficients for selected UV-vis and NIR absorption maxima (features) with well-quantified uncertainties.

2. Experimental

2.1 Materials

A custom furnace was fabricated to facilitate spectroscopic measurements at relevant temperatures up to 600 °C. The details of the furnace design and fabrication are provided in a previous publication by a collaborator [19]. A cutaway view of the spectroscopy furnace with labeled parts is shown in Figure 1. There were two notable changes in the design of the furnace used in the present work from the originally published design: (1) the use of cartridge heaters in the furnace body walls in place of the spiral resistive element below the samples, decreasing any thermal gradient in the vertical plane of the sample cuvettes, and (2) the removal of the blanking plate to simplify fabrication. The furnace contains five positions for quartz cuvettes (Lichen Cottage) on a sample holder with five-fold symmetry, allowing for the samples to be rotated into each of the five beamlines in the spectroscopy furnace. This design allows for rapid, sequential analysis of samples using different techniques or multiple sets of fiber optics for different energy ranges.

Experiments were carried out in an inert atmosphere, argon-filled gloveboxes with <1 ppm O_2 and <0.5 ppm H_2O to prevent water and oxygen contamination of the analyte salts.

The spectra were obtained from a fused LiCl-KCl eutectic salt mixture containing between 30mM and 480mM of a given rare earth trichloride analyte salt. The LiCl (Alfa Aesar, 99%) and KCl (Acros Organics, Extra Pure) were dried overnight under vacuum in a furnace at approximately 250 °C and then mixed at a 54-46 wt.% ratio (LiCl:KCl) to form the eutectic salt mixture. Ampouled anhydrous $NdCl_3$ (Alfa Aesar, 99.99% pure Ultra Dry), $SmCl_3$ (thermo scientific, ≥99.9% REO basis), $DyCl_3$ (Sigma Aldrich, 99.99% pure) were used as the analytes. The component salts were portioned using an analytical balance, mixed, and then heated at 300 °C in the cuvette for 2h in the spectroscopy furnace prior to fusion. The salt mixture was then fused at 400 °C, allowed to rest at this temperature overnight to ensure complete dissolution

of the lanthanide trichlorides, and then stirred with a quartz rod. The temperature was then raised to 500 °C and the melt was allowed to thermally equilibrate for 1h prior to spectroscopic analysis.

Absorption spectra were recorded with a Cary 5000 UV-vis-NIR spectrophotometer (Agilent Technologies, USA) with a dual beam photometric system. Incident radiation is generated by a tungsten halogen lamp for the visible and NIR ranges and a deuterium arc lamp for the UV range. To remove the absorption effects of the fiber optic cables and LiCl-KCl matrix, blank spectra were recorded at each temperature for each experiment and subtracted from the recorded spectra from the samples.

The incident radiation was transmitted into the glovebox and spectroscopy furnace using custom high-temperature fiber optic cables with hermetically sealed passthroughs and a usable range from 200 nm to 2400 nm. The incident radiation was collimated with a planar-convex lens at the terminus of the fiber, passed through the sample, and the transmitted radiation was focused with a second planar-convex lens onto the return fiber. The incident radiation and transmitted radiation were transmitted to and from the spectrophotometer using a fiber optic coupler which incorporates a rear beam balancer to account for the effects of the fiber optic coupler on the signal.

2.2 Spectrum Processing

Spectra were processed using Spectragryph (version 1.2.15), a software suite for optical spectroscopy signal processing and analysis [20]. An adaptive baseline was applied to each spectrum using the maximal coarseness possible to remove baseline fluctuations while avoiding artificial removal of any absorption feature intensity. In the case of the NIR spectrum of Nd^{3+}, a Savisky-Golay smoothing algorithm was applied to reduce noise (15 nm interval, 5^{th}-order polynomial) while preserving the profile and peak intensity of the NIR absorption feature.

2.3 Molar Absorption Coefficient Calculation

Molar absorption coefficients were determined using a weighed least-squares linear regression of the absorption maxima absorbance for the relevant transition to account for the correlated error induced in the concentration (the abscissa) and the absorption (the ordinate) [21]. A Matlab script was adapted for this calculation from a previously published method [22]. Uncertainty is reported at a 1σ confidence level.

3. Results and Discussion

The absorption spectra of Nd^{3+}, Sm^{3+}, and Dy^{3+} in LiCl-KCl eutectic were recorded in the range from 230 nm – 2400 nm (43478 cm^{-1} – 4167 cm^{-1}). The lower limit of this range is set by the limits of the spectrophotometer as absorption increases with decreasing wavelength below about 300 nm due to a combination of (I) increased Raleigh scattering, (II) decreasing transmission in the fiber optic cables, and (III) strong UV absorption attributed to charge transfer transitions in the LiCl-KCl molten salt [23]. Spectra were recorded with Nd^{3+} (UV-vis), Sm^{3+} (UV-vis-NIR), and Dy^{3+} (NIR) concentrations of 30 mM, 60 mM, 90 mM, and 120 mM and with Nd^{3+} (NIR) and Dy^{3+} (UV-vis) concentrations of 120 mM, 240 mM, 360 mM, and 480 mM. These concentration ranges were selected to be in analytically relevant regions for electrorefining operations for $NdCl_3$ and $SmCl_3$, which are present as fission products. The higher concentration range (120mM – 480 mM) for Nd^{3+} (NIR range) and Dy^{3+} (UV-vis range) were selected to increase the signal intensity for regions with transitions with low molar absorbance. The conversions of molarity to mole percentage and weight percentage for Nd^{3+}, Sm^{3+}, and Dy^{3+} are presented in Table 1 for the convenience of the reader, as these measures are all commonly used in the literature and engineering applications involving these analytes. For all figures presented in this report, spectral ranges with no observable absorption features were omitted from the plots for the sake of clarity. The assignment of hypersensitive transitions in the figures is based on the work of Henrie *et. al.* [24].

The molar absorption coefficients of selected absorption maxima in the UV, visible, and NIR ranges are tabulated in Table 2. Many of the UV and visible range molar absorption coefficients were previously determined by Kim and Yun, and their values are included for comparison to those determined in the present work [11]. The molar absorption coefficients for the NIR absorption maxima shown in Table 2 have not previously been reported.

3.1 $NdCl_3$

For Nd^{3+}, the spectra recorded in the UV, visible, and first portion of the NIR ranges are shown in Figure 2 with annotations of the excited state above each absorption feature [25]. The NIR spectra in the middle of the NIR range is shown in Figure 3. The NIR transition at ~1630 nm in Figure 3 is extremely weak in the LiCl-KCl eutectic environment but is observable, and there is a stronger transition beginning at the far NIR edge, near 2300 nm.

The absorbance spectra of Nd^{3+} in LiCl-KCl eutectic molten salt has been reported several times in literature up to about 1000 nm, and the spectra from the present work agree with the previous reports

with respect to peak position and profile [11, 12, 25]. The assignment of electronic transitions to the UV and visible range absorption features of Nd^{3+}, as well as the hypersensitive transitions, were made on the basis of those given in previous literature [11, 16, 24, 25]. The NIR spectrum above 1000 nm has not previously been reported for Nd^{3+} in LiCl-KCl eutectic molten salt or other alkali halide molten salts at any temperature.

3.1.1 Assignment of NIR absorption bands

In the present investigation, we observe a weak, broad absorption feature with the most intense maxima at ~1630 nm, shown in Figure 3. To our knowledge, this absorption feature has not been observed in any previous studies of Nd^{3+} in any solid or liquid phase [16, 26-28].

To assign the previously unobserved NIR absorption band to the electronic transition it originates from, we utilized the methods used by Chrissanthopoulos and Papatheodorou to assign the absorbance bands associated with the $^4I_{9/2} \rightarrow {}^4G_{5/2}$, $^2G_{7/2}$ electronic transitions of Nd^{3+} in LiCl-KCl eutectic based on analysis of the crystal field levels calculated by Foster and coworkers for Nd^{3+} in the Y-based elpasolite [25]. Their assignments are shown in Figure 4 overlaid on the absorbance spectra from the present work. The energies of the same crystal field levels calculated by Tanner *et. al.* for Nd^{3+} in Gd-based elpasolite are added to the figure for additional context showing the extension of the possible range of energies from the two sets of data [16, 25, 26]. This analysis of the well-characterized $^4I_{9/2} \rightarrow {}^4G_{5/2}$, $^2G_{7/2}$ absorbance feature shows the utility of assigning electronic transitions and crystal field levels from lanthanide elpasolite spectra to high-temperature trivalent lanthanides in LiCl-KCl eutectic molten salt and supports our assignments of the electronic multiplet level and crystal field levels to this newly observed NIR absorption feature.

We have assigned the NIR absorbance feature to the electronic transition from the $^4I_{9/2}$ ground state to the $^4I_{15/2}$ multiplet. The energy of the crystal field splitting of this multiplet level in Cs_2NaYCl_6:Nd^{3+}(5 mol%) was calculated by Foster and coworkers and in $Cs_2NaGdCl_6$:Nd^{3+} (1 mol%) by Tanner and coworkers but neither investigation yielded any experimental observation of the transition [16, 26]. The crystal field levels from these calculations are shown overlaid on the experimentally observed absorption feature in Figure 5 with good agreement between the previously calculated energies for the crystal field levels for Nd^{3+} doped into Gd- and Y-based elpasolites and the peak energies of Gaussian peaks fit to the experimentally observed absorption feature based on the inflection points of the feature. While the underlying distribution of energies of the transitions to each crystal field level are not expected to be strictly Gaussian in profile, these peaks are sufficient to serve as a rough guide to the

location of the underlying crystal field levels, if not a rigorous quantitative indication of their exact position and energy distribution. Based on the crystal field energy calculations, four bands are expected and these four bands are evident within the absorbance feature in Figure 5 in the vicinity of the expected energy ranges.

The large increase in absorption that begins at ~2300 nm and increases approaching the limits of the analysis at 2400 nm most likely originates with the transition to the $^4I_{13/2}$ multiplet level. This multiplet has its highest energy crystal field energy level in the range of 2388 nm – 2425 nm in the previous elpasolite studies mentioned above [16, 26]. The fact that most of the calculated crystal field energy levels for the multiplet lie at or just beyond the edge of the analytical range of the present investigation explains the observation of only the initial shoulder of the absorption feature.

3.1.2 Molar Absorption Coefficient Determination

The molar absorption coefficients were determined for three analytically relevant absorption bands of Nd^{3+} in the visible region of the spectra. The estimates of the molar absorption coefficients for these bands in the present work compared favorably with the previous estimates of Kim and Yun [11], with less than 10% difference, but were systematically lower than the previous estimates. In the previous investigation, the reported uncertainty bands are not specified with a confidence level, and are therefore incomplete. If we assume the same confidence interval used in the present work, 1σ or 68%, the scale of the uncertainty of the present estimates are of similar magnitude to the previously reported estimates, with the exception for the estimate of the 588 nm band, where the uncertainty for the present work is one order of magnitude smaller than in the previous investigation.

The ~1630 nm NIR transition is extremely weak in the LiCl-KCl solvent, making it unsuitable for analytical use in concentration quantification in the range examined presently, up to 480 mM Nd^{3+}, as noise induced variation in the signal and baseline make accurate intensity determination difficult. Therefore, no attempt was made to determine and report the molar absorbance coefficient.

4.2 $SmCl_3$

The UV, visible, and NIR absorption spectra of Sm^{3+} in LiCl-KCl eutectic with labeled transitions are shown in Figure 6, Figure 7, Figure 8, respectively.

4.2.1 Molar Absorption Coefficient Determination

The absorption spectrum of Sm^{3+} in LiCl-KCl eutectic at 500 °C up to 1000 nm and an estimation of the molar absorption coefficient of several UV and visible range absorption bands has been reported

previously [11]. Additionally, the NIR spectrum of Sm^{3+} in LiCl-KCl eutectic at 500 °C has been reported in the NIR range but molar absorption coefficients in the NIR have not been reported to our knowledge [29]. The assignment of electronic transitions to the UV, visible, and NIR range absorption features of Sm^{3+}, as well as the hypersensitive transitions, were made on the basis of those given in previous literature [11, 24, 29].

The molar absorption coefficients estimated in the UV and visible ranges in present work compare favorably with those published previously [11]. The uncertainties for the Sm^{3+} molar absorption coefficients are approximately one order of magnitude smaller than the uncertainties for the previous estimates. The molar absorption coefficients calculated in the present work for five NIR peaks between 1245 nm and 1861 nm have not previously been reported in the literature. These molar absorption coefficients have uncertainties of a similar magnitude as the UV and visible range molar absorption coefficients and similar coefficients of determination, all $r^2 > 0.998$, suggesting that the absorption vs. concentration relationship in this range of concentration is linear with a high degree of certainty.

4.3 $DyCl_3$

The UV, visible, and NIR absorption spectra of Dy^{3+} in LiCl-KCl eutectic with labeled transitions are shown in Figure 9, Figure 10, and Figure 11.

4.3.1 Molar Absorption Coefficient Determination

The absorption spectra of $DyCl_3$ in LiCl-KCl eutectic at 500 °C up to 1000 nm and an estimation of the molar absorption coefficient of several UV and visible range absorption bands has been reported previously [11]. A limited portion of the spectrum in the NIR range has been reported from 1190 nm – 1420 nm, containing the $^6H_{15/2} \rightarrow {}^6F_{11/2}$transition, but the region from 900 nm – 2400 nm, excluding the aforementioned range, has not been reported to our knowledge [29]. The NIR region contains four transitions, including the highest intensity transition in the Dy^{3+} absorption spectrum at 1290 nm, as well as three less intense transitions, with intensities on par with the intensities of the UV and visible range transitions. The assignment of electronic transitions to the UV and visible range absorption features of Dy^{3+}, as well as the hypersensitive transitions, were made on the basis of those given in previous literature [11, 24]. The NIR features were assigned electronic transitions on the basis of an analysis of the energy levels of Dy^{3+} in $Cs_2NaDyCl_6$ elpasolite, a solid phase crystal in which the Dy^{3+} ions are in undistorted octahedral coordination with chlorine atoms, and which has been shown to correlate well with the energy levels of lanthanide ions in alkali halide molten salts [17, 25].

Like the other analytes in the present work, the molar absorption coefficients found here for the UV and visible range absorption maxima were similar to those from the previous publication [11]. The molar absorption coefficients for the four NIR Dy^{3+} transitions in LiCl-KCl eutectic have not been reported previously. The 1290 nm peak is particularly intense and is a good candidate for analytical use, especially considering the low intensity of the other absorption features, making their use for concentration determination less desirable for lower concentrations of Dy^{3+}.

5. Conclusion

We have recorded the absorption spectra of Nd^{3+}, Sm^{3+}, and Dy^{3+} from the UV range through the NIR range up to 2400 nm. Molar absorption coefficients were determined and tabulated for selected absorption maxima for these analytes in the UV, visible, and NIR ranges. The NIR absorption features observed in the present work are found to have electronic origins and to have absorption vs. concentration relationships that agree with the Beer-Lambert law, suggesting that they are suitable for analytical concentration determination and may even prove to be superior to UV and visible range absorption maxima in some cases due to greater intensity, less Rayleigh scattering, or, potentially, having fewer overlapping of features than the UV or visible ranges in cases with multiple lanthanide trichloride species present. Both Sm^{3+} and Dy^{3+} have strong hypersensitive transitions in the NIR range that are as intense or even more intense than previously characterized transitions in the UV and vis ranges, making those transitions candidates for concentration determination in molten salt in systems where they are present.

For Nd3+, we have observed a NIR absorption feature that has not previously been reported in any experimental work in any solvent or phase containing Nd3+. The feature was compared to theoretically calculated crystal field energy levels from previous work with Nd-doped elpasolite solids and the energy envelope of the absorption feature observed in the present work compared favorably with the calculated crystal field energies for octahedrally coordinated Nd3+. On this basis, the absorption feature was assigned as originating from the 4I9/2 →4I15/2 transition.

Acknowledgements

This research is being performed using funding received from the DOE Office of Nuclear Energy's Nuclear Energy University Programs under award DE-NE0008889 and the US Nuclear Regulatory Commission (USNRC) under contract 31310018M0032. Dr. Kenny Osborne and Ms. Nancy Hebron-Isreal serve as the program managers for the DOE and NRC awards, respectively.

This material is based upon work supported by the National Science Foundation Graduate Research Fellowship Program under Grant No. DGE-1447692. Any opinions, findings, and conclusions or recommendations expressed in this material are those of the author(s) and do not necessarily reflect the views of the National Science Foundation, the U.S. Department of Energy, or the United States Government.

Declaration of interests

☒ The authors declare that they have no known competing financial interests or personal relationships that could have appeared to influence the work reported in this paper.

☐ The authors declare the following financial interests/personal relationships which may be considered as potential competing interests:

Author Contributions

Jeremy Moon: Conceptualization, methodology, formal analysis, investigation, writing – original draft, visualization **Dev Chidambaram:** Conceptualization, writing – review and editing, supervision, project administration, funding acquisition

References

[1] N. Tsoulfanidis, *The Nuclear Fuel Cycle*, 1st ed. La Grange Park, Il: American Nuclear Society, 2013.

[2] M. A. Williamson and J. L. Willit, "Pyroprocessing Flowsheets for Recycling Used Nuclear Fuel," *Nuclear Engineering and Technology,* vol. 43, no. 4, pp. 329-334, 2011-08-01 2011, doi: 10.5516/NET.2011.43.4.329.

[3] J. J. Laidler, J. E. Battles, W. E. Miller, J. P. Ackerman, and E. L. Carls, “Development of pyroprocessing technology,” *Progress in Nuclear Energy*, vol. 31, no. 1, pp. 131–140, Jan. 1997, doi: 10.1016/0149-1970(96)00007-8.

[4] C. C. McPheeters, R. D. Pierce, and T. P. Mulcahey, “Application of the pyrochemical process to recycle of actinides from LWR spent fuel,” *Progress in Nuclear Energy*, vol. 31, no. 1, pp. 175–186, Jan. 1997, doi: 10.1016/0149-1970(96)00010-8.

[5] P. Baron *et al.*, “A review of separation processes proposed for advanced fuel cycles based on technology readiness level assessments,” *Progress in Nuclear Energy*, vol. 117, p. 103091, Nov. 2019, doi: 10.1016/j.pnucene.2019.103091.

[6] T. Y. Karlsson, G. L. Fredrickson, T.-S. Yoo, D. Vaden, M. N. Patterson, and V. Utgikar, "Thermal analysis of projected molten salt compositions during FFTF and EBR-II used nuclear fuel

processing," (in en), *Journal of Nuclear Materials,* vol. 520, pp. 87-95, July 1, 2019 2019, doi: 10.1016/j.jnucmat.2019.04.016.

[7] T. Inoue and L. Koch, "Development of pyroprocessing and its future direction," *Nuclear Engineering and Technology,* vol. 40, no. 3, pp. 183-190, 2008-04-01 2008.

[8] J.-C. G. Bünzli and S. V. Eliseeva, "Basics of Lanthanide Photophysics," in *Lanthanide Luminescence: Photophysical, Analytical and Biological Aspects*, P. Hänninen and H. Härmä Eds., (Springer Series on Fluorescence. Berlin, Heidelberg: Springer, 2011, pp. 1-45.

[9] T. G. Mayerhöfer, S. Pahlow, and J. Popp, "The Bouguer-Beer-Lambert Law: Shining Light on the Obscure," (in en), *ChemPhysChem,* vol. 21, no. 18, pp. 2029-2046, 2020 2020, doi: 10.1002/cphc.202000464.

[10] C. A. Schroll, A. M. Lines, W. R. Heineman, and S. A. Bryan, "Absorption spectroscopy for the quantitative prediction of lanthanide concentrations in the 3LiCl–2CsCl eutectic at 723 K," (in en), *Analytical Methods,* vol. 8, no. 43, pp. 7731-7738, 2016-11-03 2016, doi: 10.1039/C6AY01520D.

[11] B. Y. Kim and J.-I. Yun, "Optical absorption and fluorescence properties of trivalent lanthanide chlorides in high temperature molten LiCl–KCl eutectic," (in en), *Journal of Luminescence,* vol. 178, pp. 331-339, October 1, 2016 2016, doi: 10.1016/j.jlumin.2016.06.010.

[12] C. V. Banks, M. R. Heusinkveld, and J. W. O'Laughlin, "Absorption Spectra of the Lanthanides in Fused Lithium Chloride-Potassium Chloride Eutectic," (in en), *Analytical Chemistry,* vol. 33, no. 9, pp. 1235-1240, 1961-08-01 1961, doi: 10.1021/ac60177a032.

[13] T. Fujii, H. Moriyama, and H. Yamana, "Electronic absorption spectra of lanthanides in a molten chloride: I. Molar absorptivity measurement of neodymium(III) in molten eutectic mixture of LiCl–KCl," (in en), *Journal of Alloys and Compounds,* vol. 351, no. 1, pp. L6-L9, March 10, 2003 2003, doi: 10.1016/S0925-8388(02)01081-2.

[14] W. T. Carnall, P. R. Fields, and K. Rajnak, "Electronic Energy Levels in the Trivalent Lanthanide Aquo Ions. I. Pr3+, Nd3+, Pm3+, Sm3+, Dy3+, Ho3+, Er3+, and Tm3+," *The Journal of Chemical Physics,* vol. 49, no. 10, pp. 4424-4442, November 15, 1968 1968, doi: 10.1063/1.1669893.

[15] W. T. Carnall, P. R. Fields, and K. Rajnak, "Spectral Intensities of the Trivalent Lanthanides and Actinides in Solution. II. Pm3+, Sm3+, Eu3+, Gd3+, Tb3+, Dy3+, and Ho3+," *The Journal of Chemical Physics,* vol. 49, no. 10, pp. 4412-4423, November 15, 1968 1968, doi: 10.1063/1.1669892.

[16] D. R. Foster, F. S. Richardson, and R. W. Schwartz, "Optical spectra and crystal field analysis of Nd3+ in the cubic Cs2NaYCl6 host," *The Journal of Chemical Physics,* vol. 82, no. 2, pp. 601-617, January 15, 1985 1985, doi: 10.1063/1.448535.

[17] D. R. Foster and F. S. Richardson, "Optical spectra and crystal field analysis of Dy3+ in Cs2NaDyCl6 and Cs2NaYCl6:Dy3+ (5 mol %)," (in en), *The Journal of Chemical Physics,* vol. 82, no. 3, pp. 1085-1101, 1985/02// 1985, doi: 10.1063/1.448481.

[18] A. K. Banerjee and R. W. Schwartz, "The optical absorption and emission spectra of Cs2NaSmCl6," (in en), *Chemical Physics,* vol. 58, no. 2, pp. 255-266, June 15, 1981 1981, doi: 10.1016/0301-0104(81)80061-4.

[19] W. C. Phillips *et al.*, "Design and performance of high-temperature furnace and cell holder for in situ spectroscopic, electrochemical, and radiolytic investigations of molten salts," (in en), *Review of Scientific Instruments,* vol. 91, no. 8, p. 083105, 2020/08/14/ 2020, doi: 10.1063/1.5140463.

[20] *Spectragryph - optical spectroscopy software*. (2022).

[21] D. York, N. M. Evensen, M. L. Martínez, and J. De Basabe Delgado, "Unified equations for the slope, intercept, and standard errors of the best straight line," *American Journal of Physics,* vol. 72, no. 3, pp. 367-375, 2004/03// 2004, doi: 10.1119/1.1632486.

[22] K. Thirumalai, A. Singh, and R. Ramesh, "A MATLAB(TM) code to perform weighted linear regression with (correlated or uncorrelated) errors in bivariate data," (in English), *Journal of the Geological Society of India,* vol. 77, no. 4, pp. 377-380, 2011/04// 2011, doi: http://dx.doi.org/10.1007/s12594-011-0044-1.

[23] L. E. Orgel, "Charge-transfer spectra and some related phenomena," (in en), *Q. Rev. Chem. Soc.,* vol. 8, no. 4, pp. 422-450, 1954/01/01/ 1954, doi: 10.1039/QR9540800422.

[24] D. E. Henrie, R. L. Fellows, and G. R. Choppin, "Hypersensitivity in the electronic transitions of lanthanide and actinide complexes," (in en), *Coordination Chemistry Reviews,* vol. 18, no. 2, pp. 199-224, February 1, 1976 1976, doi: 10.1016/S0010-8545(00)82044-5.

[25] A. Chrissanthopoulos and G. N. Papatheodorou, "Temperature dependence of the f←f hypersensitive transitions of Ho3+ and Nd3+ in molten salt solvents and the structure of the LaCl3–KCl melts," (in en), *Journal of Molecular Structure,* vol. 782, no. 2, pp. 130-142, January 23, 2006 2006, doi: 10.1016/j.molstruc.2005.08.003.

[26] P. A. Tanner, J. Quagliano, and F. S. Richardson, "Luminescence and excitation spectra of Nd3+ in Cs2NaGdCl6 : NdCl3–6," (in en), *Journal of the Chemical Society, Faraday Transactions,* vol. 87, no. 11, pp. 1707-1714, 1991/01/01/ 1991, doi: 10.1039/FT9918701707.

[27] M. Deepa, R. Doddoji, C. S. D. Viswanath, and A. V. Chandrasekhar, "Optical and NIR luminescence spectral studies: Nd3+-doped borosilicate glasses," (in en), *Journal of Luminescence,* vol. 213, pp. 191-196, 2019/09/01/ 2019, doi: 10.1016/j.jlumin.2019.05.014.

[28] Y. Tian, J. Zhang, X. Jing, and S. Xu, "Optical absorption and near infrared emissions of Nd3+ doped fluorophosphate glass," (in en), *Spectrochimica Acta Part A: Molecular and Biomolecular Spectroscopy,* vol. 98, pp. 355-358, 2012/12/01/ 2012, doi: 10.1016/j.saa.2012.08.047.

[29] T. Fujii, T. Nagai, A. Uehara, and H. Yamana, "Electronic absorption spectra of lanthanides in a molten chloride: III. Absorption characteristics of trivalent samarium, dysprosium, holmium, and erbium in various molten chlorides," (in en), *Journal of Alloys and Compounds,* vol. 441, no. 1, pp. L10-L13, 2007/08/30/ 2007, doi: 10.1016/j.jallcom.2006.09.113.

Figures

Table 1: Equivelent molarity, mole percentage, and weight percentage of the analytes in the LiCl-KCl-$LnCl_3$ mixtures used in this study.

Molarity, Mole Percentage, and Weight Percentage of Analytes

	mM (mmol L^{-1})	*mol %*	*wt. %*
$NdCl_3$			
	30	0.10	0.46
	60	0.21	0.93
	90	0.31	1.39
	120	0.42	1.86
	240	0.85	3.71
	360	1.30	5.56
	480	1.76	7.42
$SmCl_3$			
	30	0.10	0.48
	60	0.21	0.95
	90	0.31	1.43
	120	0.42	1.90
$DyCl_3$			
	30	0.11	0.50
	60	0.22	1.00
	90	0.33	1.49
	120	0.44	1.99
	240	0.89	3.98
	360	1.36	5.97
	480	1.85	7.96

Table 2: Tabulation of molar absorption coefficients for the selected trivalent lanthanides. Literature values shown for comparison from Kim and Yun (2016) [11].

Molar Absorption Coefficients of Sm^{3+} Transitions at 500 °C

Peak Wavelength (nm)	Molar Absorption Coefficient, ε (L mol^{-1} cm^{-1})	r^2	Literature ε (L mol^{-1} cm^{-1})
363 nm	0.505 ± 0.005	0.9993	0.59 ± 0.03
380 nm	0.599 ± 0.005	0.9995	0.73 ± 0.05
407 nm	2.03 ± 0.01	0.9981	2.48 ± 0.10
426 nm	0.565 ± 0.005	0.9997	0.66 ± 0.02
1245 nm	0.795 ± 0.006	0.9996	-
1397 nm	0.882 ± 0.007	0.9995	-
1550 nm	1.094 ± 0.008	0.9990	-
1628 nm	0.764 ± 0.006	0.9990	-
1861 nm	0.213 ± 0.003	0.9981	-

Molar Absorption Coefficients of Nd^{3+} Transitions at 500 °C

Peak Wavelength (nm)	Molar Absorption Coefficient, ε (L mol^{-1} cm^{-1})	r^2	Literature ε (L mol^{-1} cm^{-1})
588 nm	11.47 ± 0.08	0.9995	11.9 ± 0.7
751 nm	1.74 ± 0.01	0.9992	1.89 ± 0.01
809 nm	2.33 ± 0.02	0.9990	2.51 ± 0.01

Molar Absorption Coefficients of Dy^{3+} Transitions at 500 °C

Peak Wavelength (nm)	Molar Absorption Coefficient, ε (L mol^{-1} cm^{-1})	r^2	Literature ε (L mol^{-1} cm^{-1})
301 nm	0.315 ± 0.002	0.9989	0.25 ± 0.01
352 nm	0.554 ± 0.004	0.9995	0.53 ± 0.02
389 nm	0.251 ± 0.002	0.9993	0.25 ± 0.01
455 nm	0.146 ± 0.001	0.9999	0.17 ± 0.01
912 nm	0.170 ± 0.001	0.9980	-
1111 nm	0.233 ± 0.002	0.9980	-
1290 nm	2.66 ± 0.02	0.9992	-
1760 nm	0.240 ± 0.004	0.9997	-

*all uncertainties in the present work reported as 1σ confidence intervals

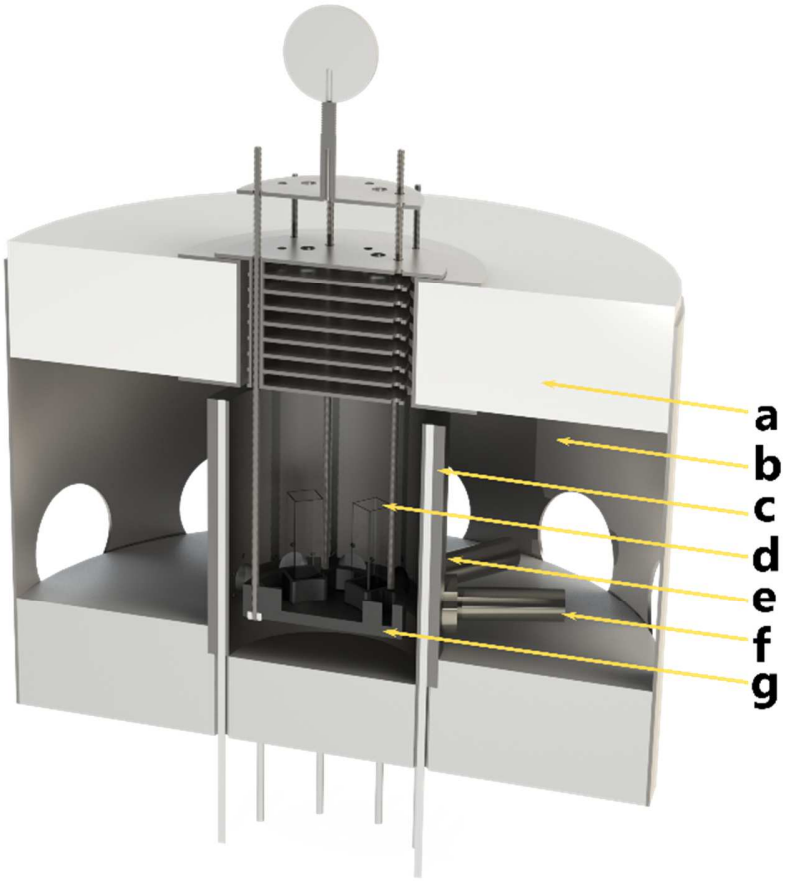

Figure 1: Spectroscopy furnace cutaway showing internal structure. a: calcium silicate rigid insulation (also on bottom, not labeled) b: fiber insulation (no pictured, fills gap between exterior and interior wall) c: resistive cartridge heater d: quartz cuvette e: furnace body f: optical port (1 of 10 total ports arranged circumferentially around the furnace body) g: sample rack. This arrangement allows for 5 individual cuvettes and 5 transmission beampaths across the furnace. Each cuvette can be rotated into each individual beampath, allowing for rapid, sequential analysis of the samples.

$NdCl_3$

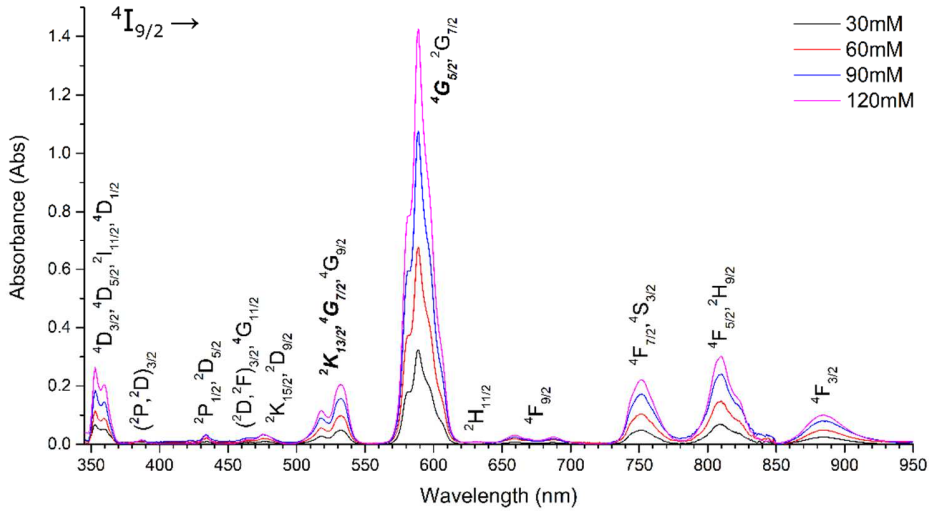

Figure 2: The absoprtion spectra of Nd^{3+} in LiCl-KCl eutectic at 500 °C from 340 nm – 950 nm. The ground state of Nd^{3+} is $^4I_{9/2}$ and the excited states of the transitions are labeled above their respective absorption features. The hypersensitive $^2K_{13/2}$, $^4G_{7/2}$, and $^4G_{5/2}$ transitions are annotated in bold. Absorption spectra for 30 mM – 120 mM are shown.

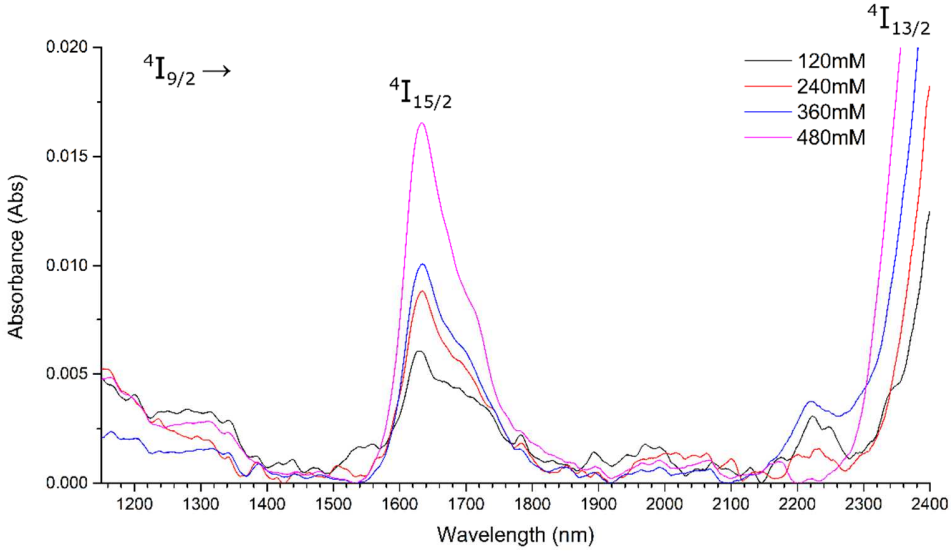

Figure 3: The absoprtion spectra of Nd^{3+} in LiCl-KCl eutectic at 500 °C from 1180 nm – 2400 nm. The ground state of Nd^{3+} is $^4I_{9/2}$ and the excited states of the transitions are labeled above their respective absorption features. Absorption spectra for 120 mM – 480 mM are shown.

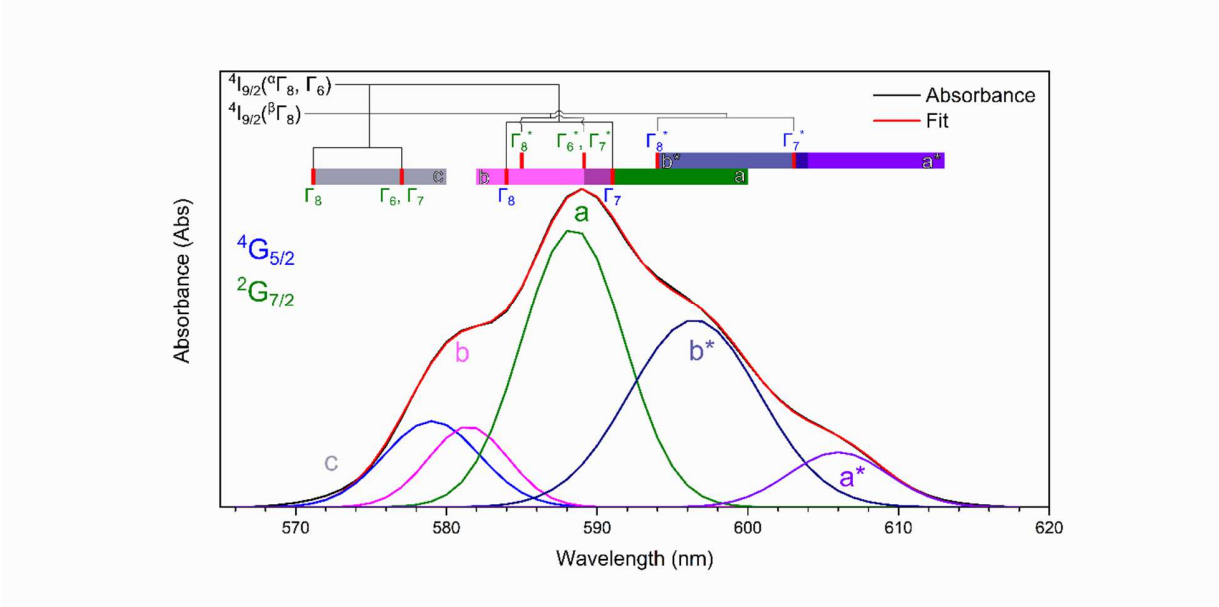

Figure 4: The Nd^{3+} absorption feature originating with the electronic transition from the $^4I_{9/2}$ ground state to the $^4G_{5/2}$ and $^2G_{7/2}$ multiplets. Five underlying bands of the Nd^{3+} absorption feature in LiCl-KCl eutectic molten salt were identified by Crissanthopoulos and Papatheodorou (based on energy calculations by Foster et. al.). Bands a, b, and c originate from the ground state crystal field levels $^\alpha\Gamma_8$ and Γ_6 and a and b* are hot bands originating from the $^\beta\Gamma_8$ crystal field level of the ground electronic state [13, 22]. The colored bard overlaying the absorption spectra represent the range of energies of the crystal field levels from previously published calculations; the energy of the crystal field levels calculated by Foster et. al. for Nd^{3+} in a Y-based elpasolite form the lower wavelength bound and those calculated by Tanner et. al. for Nd^{3+} in a Gd-based elpasolite form the upper wavelength boundary [13, 23]. The specific energies identified by foster and used by Crissanthopoulos and Papatheodorou in their analysis are annotated by vertical bars and the associated irrep of the crystal field energy level. Gaussian peaks based on the location of inflection points on the feature were fit as a guide to the eye for the probably center of gravity of each underlying band. This analysis establishes the utility of the elpasolite-based crystal field energy level calculations for the assignment of electronic origins to trivalent lanthanide absorption features in LiCl-KCl eutectic molten salt.*

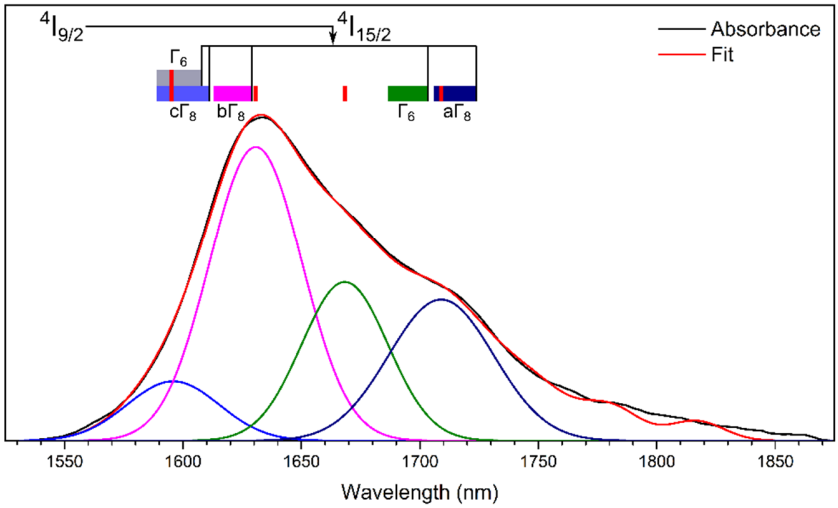

Figure 5: The NIR Nd^{3+} absorption feature between 1550 nm and 1850 nm, which has not previously been experimentally observed. A similar analysis to the that shown in Fig. 4 was carried out to enable comparison of the feature to previous energy level calculations of Nd^{3+} in Gd- and Y-based elpasolites. Gaussian peaks were fit to the major inflection points of the absorption feature to guide the eye and suggest the location of center of gravity of each underlying crystal field energy level. The calculated energies of the crystal field levels are annotated as bars over the feature with the lower bound being the energies calculated by Foster et. al. for Nd^{3+} (~5 mol%) doped into a Y-based elpasolite and the upper bound being the energies calculated by Tanner et. al. for Nd^{3+} (1 mol%) doped into a Gd-based elpasolite. The peak energies of the fitted peaks from the experimentally observed feature are annotated on the calculated energy bars, showing the relationship between the observed and calculated energies. The agreement between the previously calculated energies and the observed position of both the entire absorption feature as well as the individual crystal field levels gives us a high level of confidence in assigning this transition as the $^4I_{9/2} \rightarrow {}^4I_{15/2}$ electronic transition.

$SmCl_3$

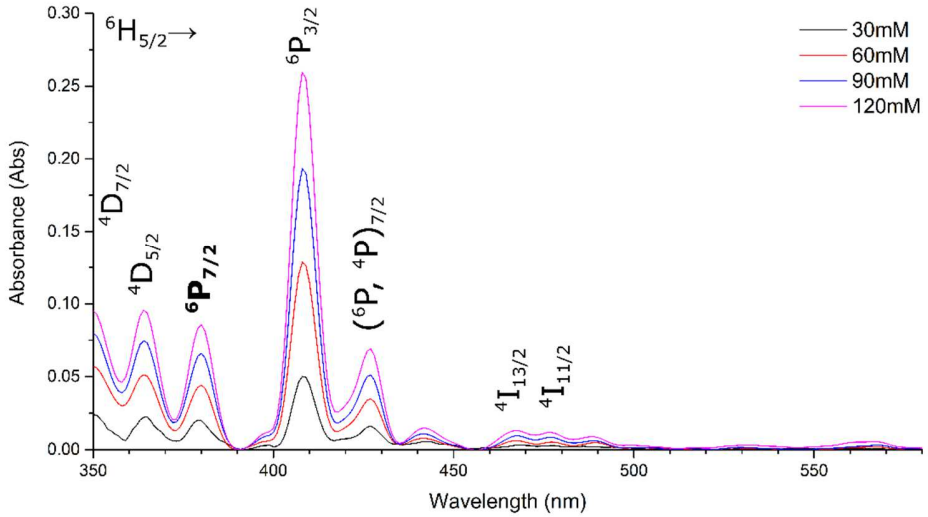

Figure 6: The absoprtion spectra of Sm^{3+} in LiCl-KCl eutectic at 500 °C from 350 nm – 580 nm. The ground state of Sm^{3+} is $^6H_{5/2}$ and the excited states of the transitions are labeled above their respective absorption features. The hypersensitive $^6P_{7/2}$ transition is annotated in bold. Absorption spectra for 30 mM – 120 mM are shown.

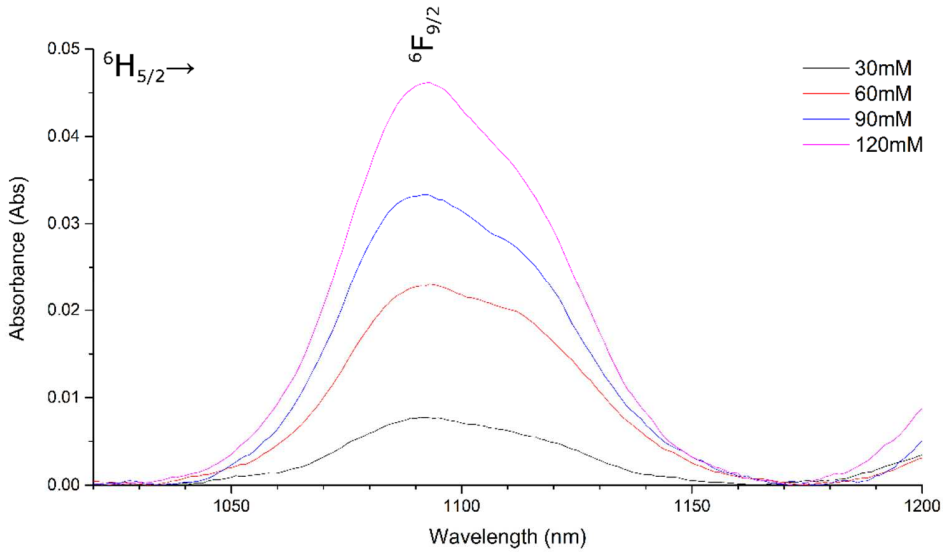

Figure 7 The absoprtion spectra of Sm^{3+} in LiCl-KCl eutectic at 500 °C from 10200 nm – 1200 nm. The ground state of Sm^{3+} is $^6H_{5/2}$ and the excited states of the transitions are labeled above their respective absorption features. Absorption spectra for 30 mM – 120 mM are shown.

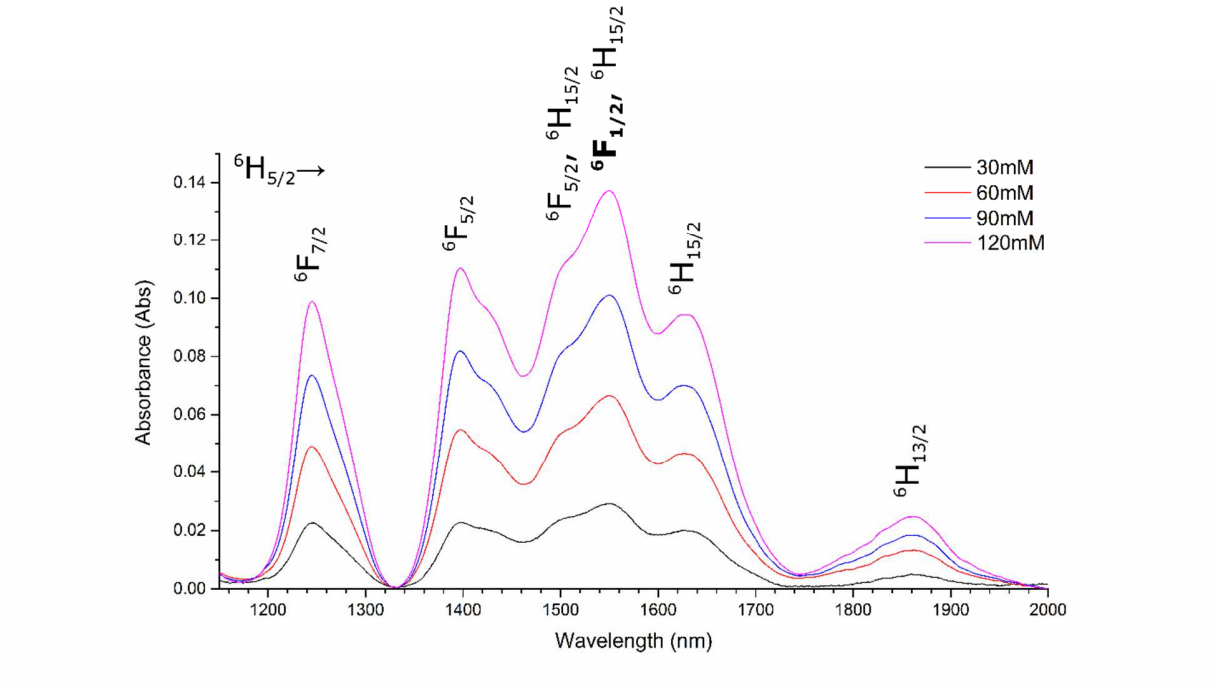

Figure 8: The absoprtion spectra of Sm^{3+} in LiCl-KCl eutectic at 500 °C from 1180 nm – 2000 nm. The ground state of Sm^{3+} is $^6H_{5/2}$ and the excited states of the transitions are labeled above their respective absorption features. The hypersensitive $^6F_{1/2}$ transition is annotated in bold. Absorption spectra for 30 mM – 120 mM are shown.

DyCl

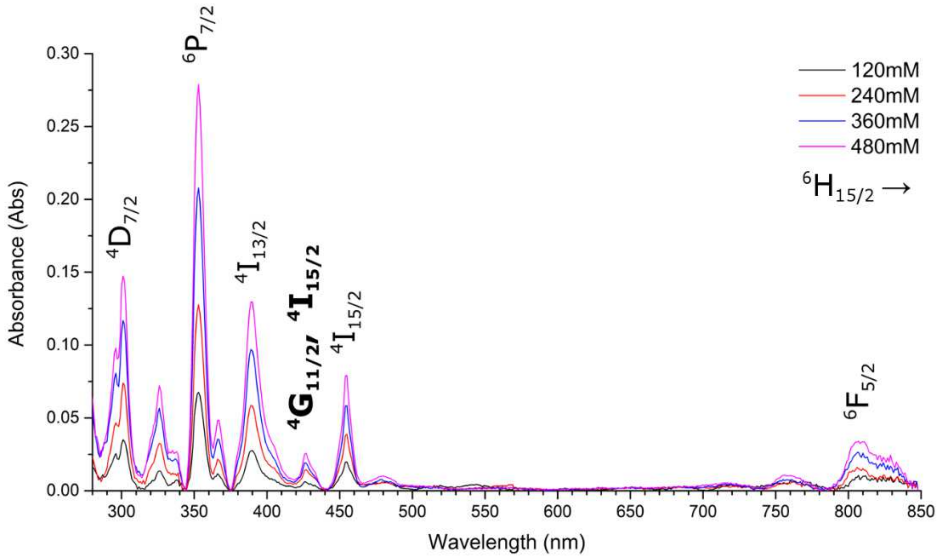

Figure 9 The absoprtion spectra of Dy^{3+} in LiCl-KCl eutectic at 500 °C from 280 nm – 850 nm. The ground state of Dy^{3+} is $^6H_{15/2}$ and the excited states of the transitions are labeled above their respective absorption features. The hypersensitive $^4G_{11/2}$ and $^4I_{15/2}$ transitions are annotated in bold. Absorption spectra for 120 mM – 480 mM are shown.

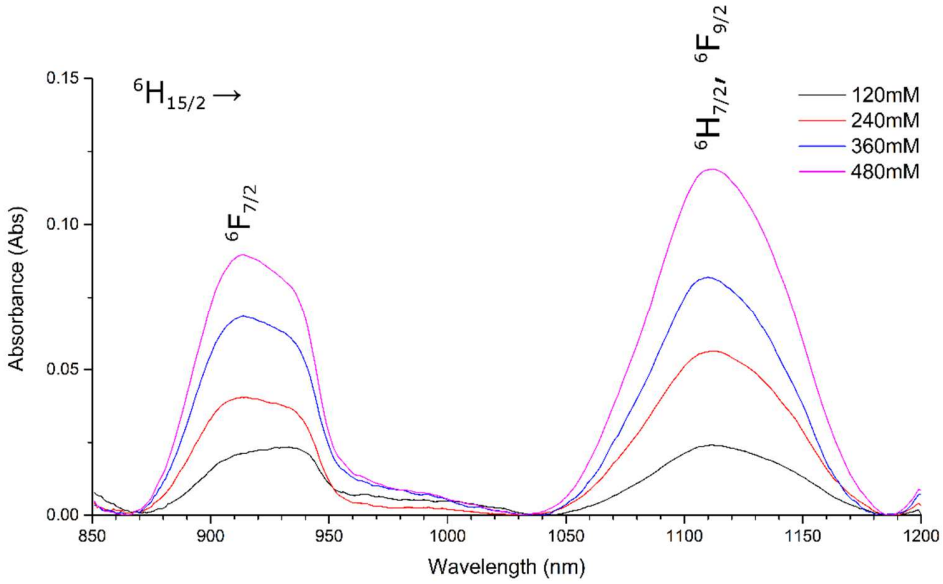

Figure 10: The absoprtion spectra of Dy^{3+} in LiCl-KCl eutectic at 500 °C from 850 nm – 1200 nm. The ground state of Dy^{3+} is $^6H_{15/2}$ and the excited states of the transitions are labeled above their respective absorption features. Absorption spectra for 120 mM – 480 mM are shown.

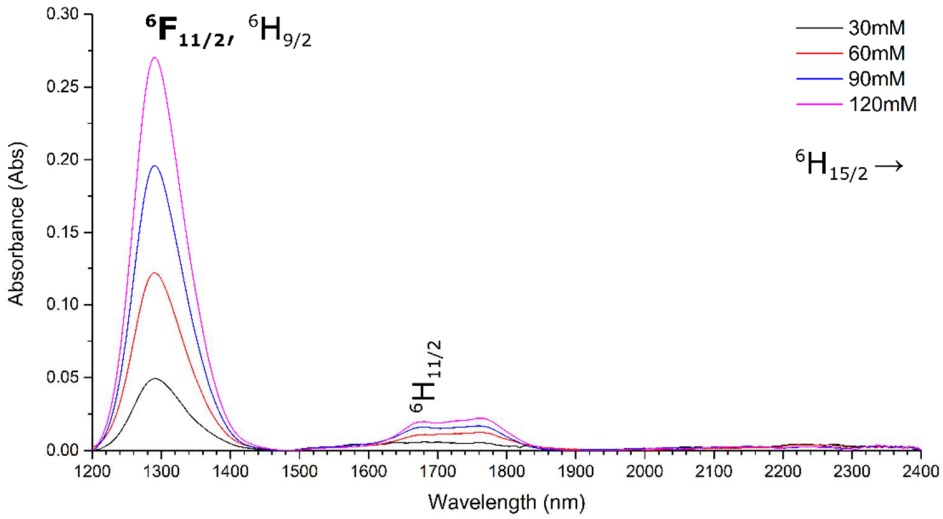

Figure 11: The absoprtion spectra of Dy^{3+} in LiCl-KCl eutectic at 500 °C from 1200 nm – 2400 nm. The ground state of Dy^{3+} is $^6H_{15/2}$ and the excited states of the transitions are labeled above their respective absorption features. The hypersensitive $^6F_{11/2}$ transition is annotated in bold. Absorption spectra for 120 mM – 480 mM are shown.